JOURNAL OF MATERIALS SCIENCE 28 (1993) 4571–4577

The interaction between proeutectoid ferrite and austenite during the isothermal transformation of two low-carbon steels – a new model for the decomposition of austenite

J.-W. LEE
Thomas J. Watson Research Center, P.O. Box 218, Yorktown Heights, NY 10598, USA

S.W. THOMPSON
Advanced Steel Processing and Products Research Center, Department of Metallurgical Engineering, Colorado School of Mines, CO 80401, USA

R. VARUGHESE, P.R. HOWELL
Department of Materials Science and Engineering, The Pennsylvania State University, University Park, PA 16802, USA

Both scanning electron microscopy (SEM) and transmission electron microscopy (TEM) have been employed to examine the austenite to proeutectoid ferrite and ferrite/carbide reactions in two low-carbon (0.04 wt%) steels. It is demonstrated that proeutectoid ferrite (both polygonal and Widmanstätten) can "partition" the prior austenite grains into several smaller units or pools. It is also shown that prior to the initiation of the pearlite reaction, ferrite grain growth can occur. The pools of austenite exert a Zener-like drag force on the migrating ferrite grain boundaries. However, the ferrite boundaries can eventually break away and small pools of austenite become completely embedded in single proeutectoid ferrite grains. Subsequently, these small pools of austenite transform to discrete regions of cementite, together with epitaxial ferrite. Conversely, certain small pools remain in contact with the ferrite grain boundaries and it is considered that transformation of these latter pools will eventually lead to the formation of massive films of cementite at the ferrite grain boundaries. Larger pools of austenite prevent ferrite boundary breakaway, and these latter, austenitic regions eventually transform to pearlite.

1. Introduction

In a previous study of two low-carbon (0.04 wt %) lamination steels, the isothermal decomposition of austenite was investigated [1] and the formation of pearlite and massive films of cementite was considered in detail. However, the proeutectoid ferrite reaction received little attention. A subsequent re-examination of the early stages of the decomposition of austenite (i.e. prior to the onset of the pearlite reaction) in these alloys has revealed a complex distribution of the remaining pools of austenite. For example, neither the size nor the location of the austenite pools could be reconciled with the conventional model, that proeutectoid ferrite nucleates on the austenite grain boundaries and forms a skeleton at the prior austenite grain boundaries: the pearlite reaction then occurs when the remaining austenite attains the eutectoid composition.

In view of this, the present work was concerned primarily with the proeutectoid ferrite reaction in two low-carbon lamination steels. In particular, the interaction between proeutectoid ferrite and the remaining pools of austenite has been documented. From this, new models for the decomposition of austenite are presented here. These models can successfully account for the observation of both films of cementite at ferrite grain boundaries and of discrete precipitates of cementite within the ferritic matrix.

2. Experimental procedure

The experimental materials were obtained from Inland Steel in the form of hot-rolled strip, 2.5 mm thick. The compositions of these steels are given in Table I. Specimen materials were austenitized at 1000 °C for 5 min and isothermally transformed in a salt bath followed by iced brine quenching. Details of the transformation temperatures and times are given in Lee *et al.* [1]. For both steels, the austenite grain size was approximately 100 μm.

0022–2461

TABLE I Chemical compositions of specimen materials

	C	Mn	Si	P	S	Al
Steel A	0.04	0.6	0.05	0.06	0.02	< 0.008
Steel B	0.04	0.7	0.22	0.09	0.02	0.21

Specimens for scanning electron microscopy (SEM) were prepared using standard techniques, etched in 2% nital and examined using an I.S.1 Super III A operating at 25 kV. Specimens for transmission electron microscopy (TEM) were obtained by electropolishing in a solution consisting of 5% perchloric acid in glacial acetic acid at room temperature and at a potential of 35 V. TEM was performed using either a Philips EM 300 operating at 100 kV or a Philips EM 420T operating at 120 kV. Phase identification employed both selected-area diffraction (SAD) patterns and low camera length (LCL) convergent-beam electron diffraction (CBED) patterns. LCL-CBED patterns were employed, for example, for the identification of small austenite particles in that: (i) Kikuchi lines are more readily visible in CBED patterns, and (ii) reflections from higher order Laue zones (HOLZs) can be analysed as follows.

The radius of the first order Laue zone (FOLZ), $|\boldsymbol{G}|$ as measured on a LCL-CBED pattern is [2]

$$|\boldsymbol{G}| = (2|\boldsymbol{k}|\,|\boldsymbol{H}|)^{1/2} \quad (1)$$

where $|\boldsymbol{k}| = 1/\lambda$ and $|\boldsymbol{H}|$ is the HOLZ spacing along $[u\,v\,w]$, where $[u\,v\,w]$ is parallel (or approximately parallel) to the electron beam. Hence $|\boldsymbol{H}|$ can be determined. $|\boldsymbol{H}|$ can also be calculated from

$$|\boldsymbol{H}| = \frac{p}{|[u\,v\,w]|} \quad (2)$$

where, for an fcc phase

$$p = 1 \quad \text{if } u + v + w \text{ is odd} \quad (3)$$

$$p = 2 \quad \text{if } u + v + w \text{ is even} \quad (4)$$

and for a bcc phase

$$p = 2 \quad \text{in } u\ v\ w \text{ are all odd} \quad (5)$$

$$p = 1 \quad \text{otherwise} \quad (6)$$

and $|[u\,v\,w]|$ is the modulus of the real-space vector along $\boldsymbol{H}$. Hence, the measured (Equation 1) and calculated (Equation 2) values of $|\boldsymbol{H}|$ can be compared and crystal structure information may be obtained routinely from single CBED patterns.

3. Results

3.1. The austenite to proeutectoid ferrite reaction

Fig. 1 is an SEM image of Steel A which had been isothermally transformed at 575 °C for 60 s. (The phenomena discussed with respect to this, and the other figures presented, are general. Hence, for subsequent micrographs, the transformation temperatures and times will be given in the figure captions only.) The

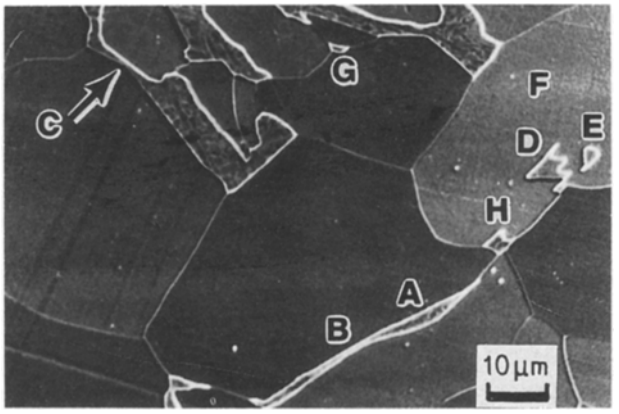

Figure 1 Scanning electron micrograph of the ferrite/austenite microstructure that develops in Steel B after 5 min at 625 °C. Note that the majority of the austenite transforms to martensite during the quench and this yields a molted appearance. Details of the microstructures are given in the text.

austenite, most of which transforms to martensite during the quench, can be differentiated from the proeutectoid ferrite, because:

(i) the martensite/austenite is attacked less readily than the ferrite. Hence, strong topographic contrast is obtained from the martensite/ferrite interfaces (Fig. 1);

(ii) the substructure within the martensite is often etched lightly so that these regions appear mottled (Fig. 1).

Reference to Fig. 1 reveals some interesting features. For example:

(iii) austenite of a very high aspect ratio is observed, e.g. at A (The term austenite will be employed for the remainder of the text because the focus of this paper is on the high-temperature phase transformations, i.e. austenite to ferrite and carbide, and not the austenite to martensite transformation which occurs during the quench.);

(iv) the curvature of austenite island A in the vicinity of B is strongly suggestive of a "pinching-off" process, i.e. this island will split eventually to form two smaller islands. A second example of this latter process is arrowed, C;

(v) the observed bowing of the ferrite grain boundary in the vicinity of austenite pool D indicates that this austenite island is exerting a Zener [3, 4] drag force on the boundary and that ferrite grain growth is occurring;

(vi) austenite pool E appears to be completely embedded in the proeutectoid ferrite. This implies that ferrite grain F has enveloped this latter pool of austenite during grain growth;

(vii) a number of the austenite pools are very small. For example, pool G is only 3 μm diameter.

Fig. 2 is a further SEM image of the ferrite/austenite aggregate and shows that a series of small (~ 1 μm), austenite pools are present, both within the ferritic matrix, A, and on ferrite grain boundaries, B. It is also of interest to note that the "intragranular" islands of austenite are approximately spherical. That the features labelled A and B in Fig. 2 are indeed

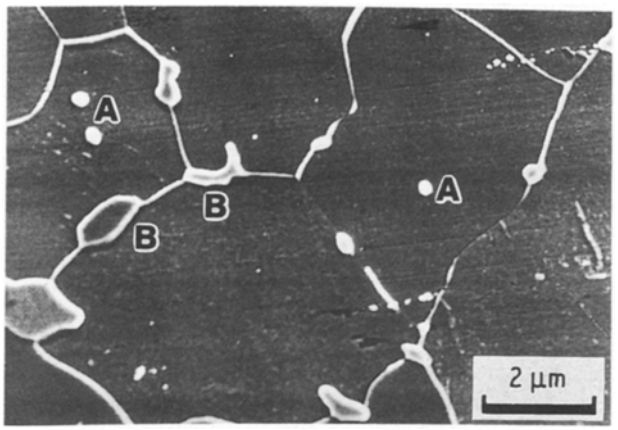

Figure 2 Scanning electron micrograph of the ferrite austenite microstructure developed in Steel B after 1 min at 575 °C.

austenite can be shown by noting that, for this specimen (Steel B; transformed for 60 s at 575 °C) no pearlite or cementite was present as confirmed by transmission electron microscopy (TEM). In addition, no other second-phase particles of similar dimensions were ever observed. In addition, the frequency with which intragranular pools of austenite were observed, rules out the possibility of these being "artefacts" due to sectioning.

Confirmation of the above was obtained using TEM. Figs 3 and 4 are examples of small pools of austenite at a ferrite grain boundary and within the ferritic matrix, respectively. The presence of stacking faults in the particles shown in Figs 3a and 4a, together with the associated diffraction patterns of Figs 3b and 4b, shows that these small pools did not transform to martensite during the quench. In Fig. 3a, the position of the grain boundary is indicative that the by-pass process is almost complete, and the austenite is almost completely embedded in proeutectoid ferrite grain B. The LCL-CBED pattern of Fig. 3b was analysed as follows. The intersection of the 400 and 022 Kikuchi lines (arrowed A and B, respectively) defined the position of the $[0\bar{1}1]_\gamma$ pole (denoted by the circle), and the position of the $[0\bar{1}1]_\gamma$ FOLZ is arrowed, C. Hence $|\boldsymbol{G}|$ could be measured (52.27 nm^{-1}) and $|\boldsymbol{H}|$ calculated (4.3 nm^{-1}). This latter calculated value compares favourably with the theoretical value of $|\boldsymbol{H}|$ $[0\bar{1}1]$ (4.0 nm^{-1}). Hence, the intergranular particle, C, in Fig. 3 can be identified unambiguously, as austenite. Although many of the small austenite particles were retained after quenching, others transformed to martensite as is shown in Fig. 5a and b. Reference to Figs 3–5 shows that the small austenite pools are either approximately spherical (Figs 4a and 5a) or are faceted (Fig. 5b). Similar

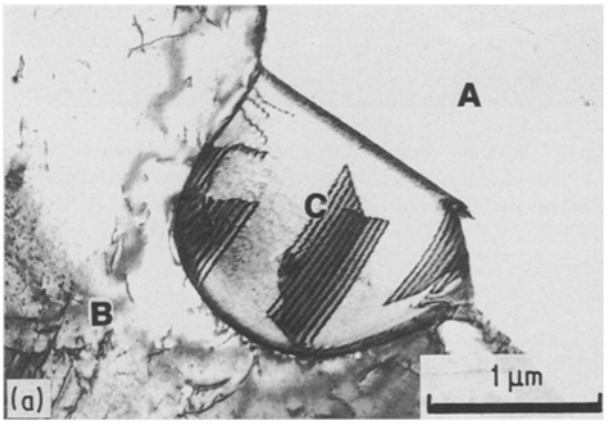

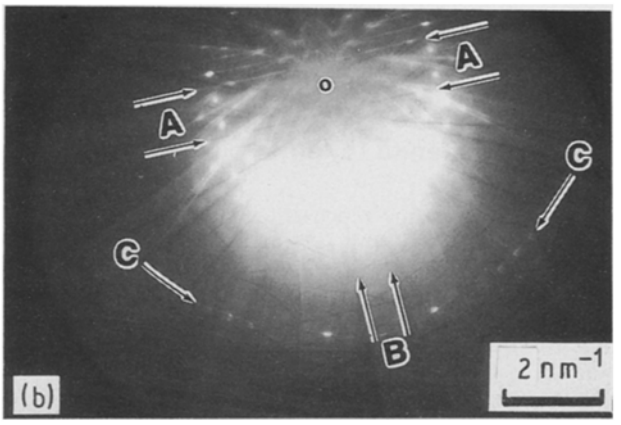

Figure 3 (a) Bright-field (BF) transmission electron micrograph of an intergranular austenite particle. Note the presence of stacking faults in the austenite (Steel B, 1 min at 575 °C). (b) Low camera length convergent-beam electron diffraction pattern from the austenite particle in Fig. 3a. See text for analysis.

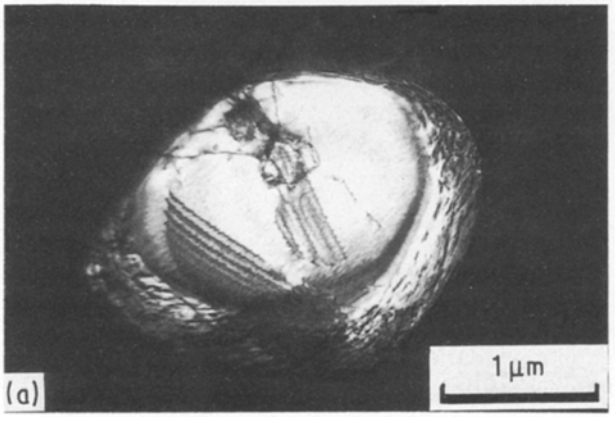

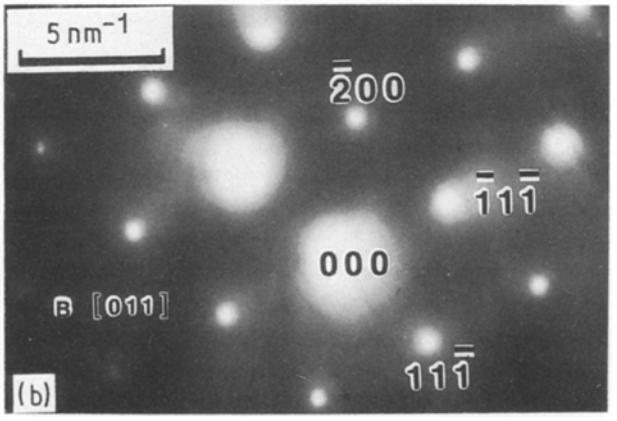

Figure 4 (a) Centered dark-field (CDF) image of an intergranular austenite particle (Steel B, 1 min at 575 °C). (b) Selected-area diffraction pattern of the austenite in (a).

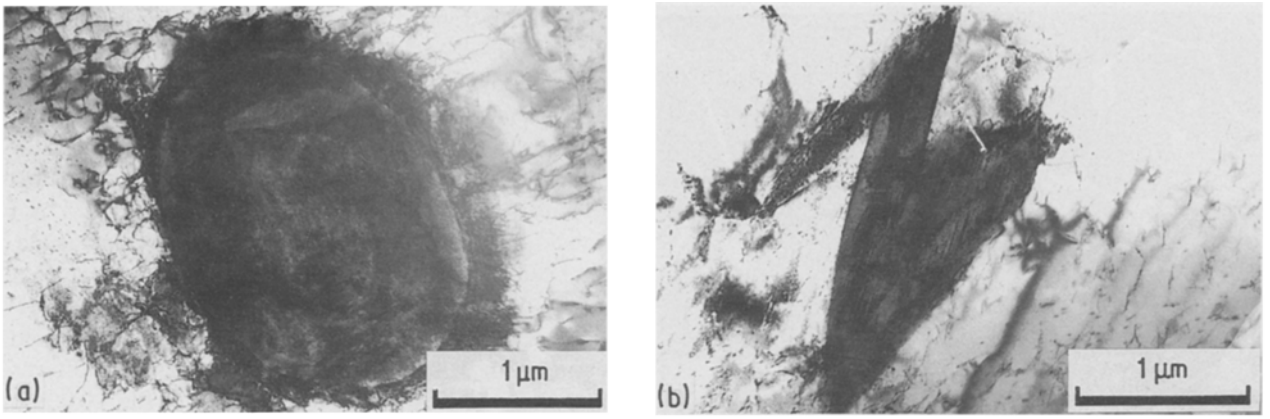

Figure 5 BF images of intragranular islands of austenite which transformed to martensite during the quench. (a) Steel B, 30 s at 675 °C. (b) Steel B, 10 s at 650 °C.

morphologies were documented using the SEM, i.e. faceted (at D, E and H in Fig. 1) and spherical (at A, Fig. 2). For the small intergranular particles, faceted interfaces were observed in association with one abutting ferrite grain (A, Fig. 3a). However, smoothly curved interfaces frequently were observed with respect to the second ferrite grain (B, Fig. 3a). The implications of these observations are deferred to the discussion.

In contrast with many of the small pools, larger pools of austenite always transformed to martensite on quenching. This is consistent with a number of earlier studies [5–8].

3.2. The austenite to ferrite plus carbide reactions

In this section, some representative examples of fully transformed, i.e. ferrite/carbide aggregates, structures are presented. Further details are given in Lee *et al.* [1]. Fig. 6 shows a relatively large (~ 30 μm long) pearlite nodule. However, discrete particles of cementite are observed in the ferritic matrix, e.g. at A (for this transformation schedule, no retained austenite was observed). Fig. 7 presents a further example of a moderately large pearlite colony in fully transformed specimen material. However, in addition to pearlite,

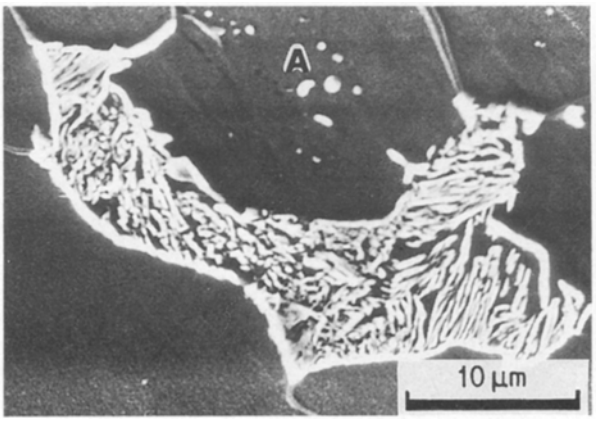

Figure 6 Scanning electron micrograph of ferrite and pearlite. Note also the intragranular cementite particles (Steel A, 30 min at 550 °C).

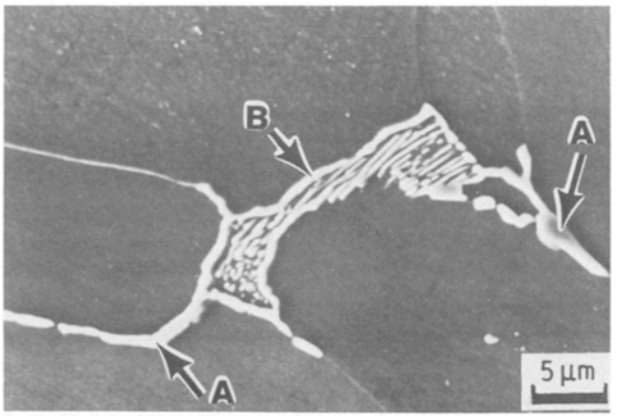

Figure 7 Scanning electron micrograph of ferrite and pearlite. Massive films of cementite are observed at proeutectoid ferrite/pearlite interfaces and at ferrite/ferrite grain boundaries (Steel A, 15 h at 650 °C).

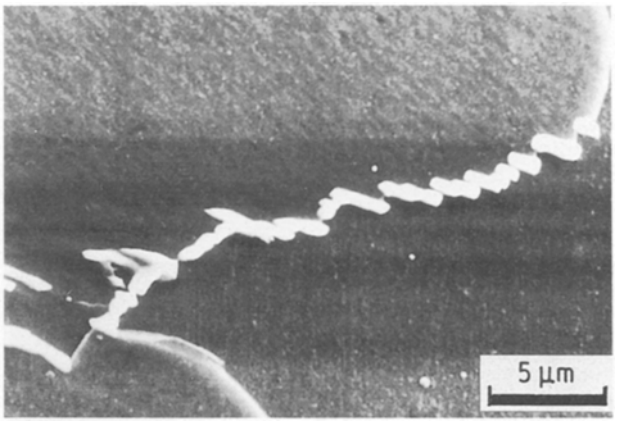

Figure 8 Scanning electron micrograph of cementite precipitates at a ferrite grain boundary (Steel B, 1 h at 625 °C).

massive films of cementite are observed on the ferrite grain boundaries (arrowed, A) and at proeutectoid ferrite pearlite/interfaces (arrowed, B). Finally, Fig. 8 shows "discrete" precipitates of cementite on a ferrite grain boundary. These precipitates are associated with "puckering" of the grain boundary.

In the following section, these observations concerning the ferrite/carbide aggregates will be discussed in relation to the results presented in Section 3.1 and new models for the decomposition of austenite will be presented.

4. Discussion

4.1. Encapsulation of austenite by ferrite

The results presented in Section 3.1 suggest that:

(i) the prior austenite grains can be partitioned by proeutectoid ferrite;

(ii) the resultant small pools of austenite exert a drag force on the migrating ferrite grain boundaries;

(iii) the ferrite grain boundaries can eventually breakaway, leading to intragranular austenite.

A possible sequence of events which will lead to the encapsulation of small pools of austenite is shown in Fig. 9. Initially it is assumed that shape instabilities develop at the austenite/ferrite interface (Fig. 9a); a number of these shape instabilities are arrowed on Fig. 10 and see Fig. 1, at B. Although the origin of these shape instabilities is uncertain, they may be formed in a manner which is similar to that discussed by Shewmon [9], i.e. they are incipient Widmanstätten side plates. Enhanced diffusion of carbon away from the protrusions will then lead to "pinching off," which will yield discrete pools of austenite at the ferrite grain boundary (Fig. 9b). A particularly striking example of the "pinching-off" process is given in Fig. 11 where it can be seen that at least three discrete regions (A, B, C) are forming from one original pool of austenite. A further example is provided in Fig. 1 where particles D, E and H are faceted and each particle displays at least one mutually parallel facet. This is strong evidence that these latter particles have identical crystallographic orientations, i.e. they formed from the same prior austenite grain.

Once the ferrite grain boundary has been created (Fig. 9b) it is subjected to normal grain-growth forces and individual boundaries will migrate towards their centres of curvature. This driving force for grain growth, will be counterbalanced by the Zener drag force. However, reference to Figs 2, 3a and 5, for example, shows that the driving force frequently outweighs the restraining force, and hence the ferrite boundaries will move around the austenite particles and finally break free. When the boundary breaks free, the austenite particle remains embedded in the ferrite matrix. These latter two stages are shown schematically in Fig. 9c and d in the experimental image of Fig. 12 (arrowed).

However, for all ageing times and temperatures investigated, many of the austenite pools remained at the ferrite grain boundaries. This can be explained in terms of the nature of the drag force. It is assumed, to a first approximation, that the austenite pools are spherical and of radius r, then the force, F, to remove the ferrite boundary from a single pool of austenite is given by

$$F = \pi r \gamma \tag{7}$$

where γ is the ferrite grain-boundary energy. Hence

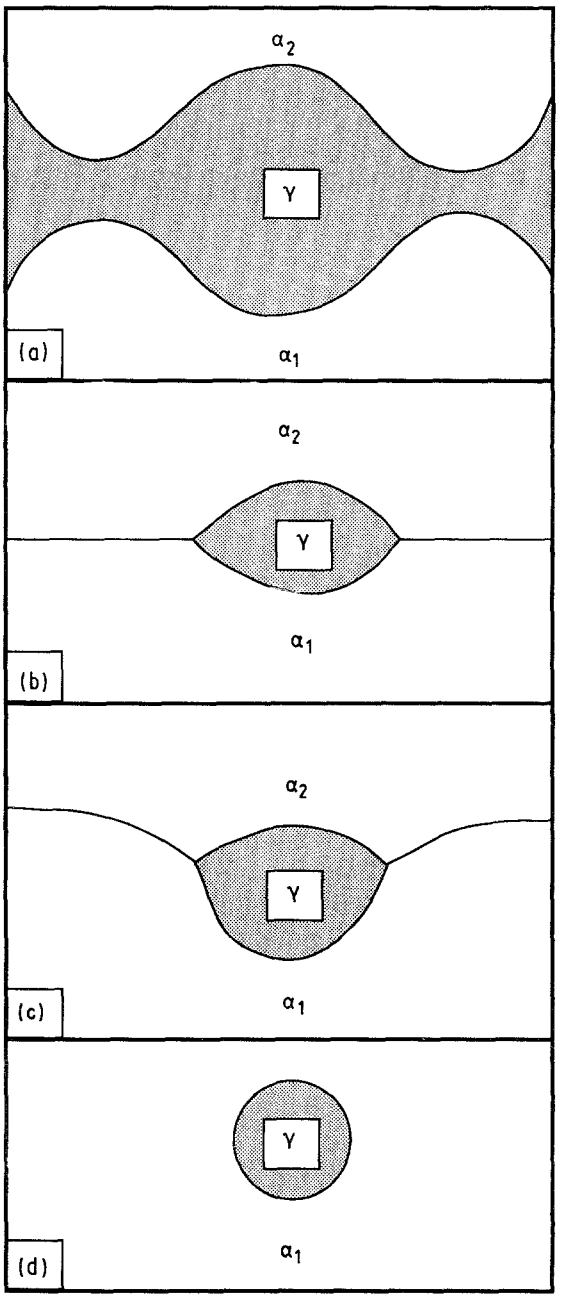

Figure 9 A schematic illustration of the formation of intragranular pools of austenite. (a) Formation of shape instabilities at the austenite/ferrite interface, which leads to (b) pinching-off of the austenite into discrete pools at ferrite grain boundaries. (c) Migration of the ferrite grain boundary around the austenite. The driving force is that for normal grain growth, leading to (d) complete encapsulation of the austenite pool in the ferritic matrix (α_1).

the large pools of austenite will exert a much larger retarding force and ferrite grain growth will be suppressed. Eventually, these large regions will transform to pearlite. This is exactly what happens as shown by the images of Figs 6 and 7.

Now, if a single, large pool of austenite of radius r_0 partitions to form N pools of austenite, each of radius r_1, then the total drag force will decrease because the total area of boundary destroyed after partitioning ($N\pi r_1^2$) will be less than that of the single, large pool of austenite, prior to partitioning (πr_0^2). This follows because the pinching-off process creates ferrite grain-boundary area due to an increase in the volume fraction of ferrite. Hence, partitioning will promote encapsulation.

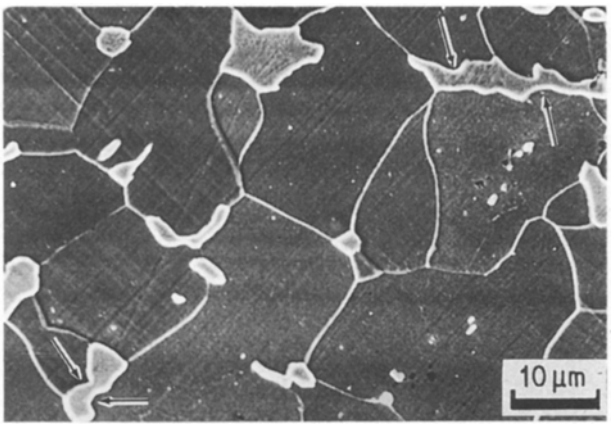

Figure 10 Scanning electron micrograph of many, small pools of austenite. For discussion, see text. (Steel B, 1 min at 575 °C).

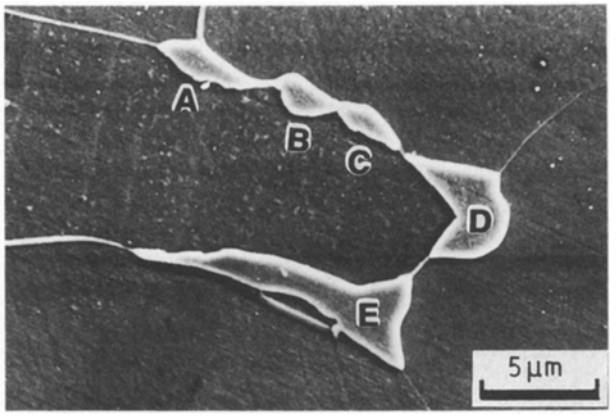

Figure 11 Scanning electron micrograph of the pinching-off process (Steel A, 1 min at 550 °C).

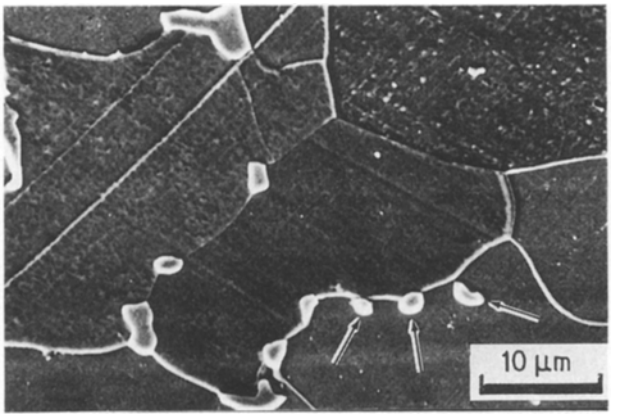

Figure 12 Scanning electron micrograph of the various stages of encapsulation (Steel B, 1 min at 550 °C).

Austenite islands A–C (Fig. 12) formed from a single prior austenite grain by a "pinching-off" process. Owing to their close proximity, it is also highly likely that pools D and E formed from the same austenite grain. This implies that a second mechanism of partitioning is operative, i.e. partitioning can occur by the preferential growth of Widmanstätten side plates (the plate-like nature of the ferrite grain in Fig. 11 substantiates this hypothesis) (A good example of partitioning by Widmanstätten side plates is also shown in Fig. 1 of Lee *et al.* [1].) It should be noted that this latter mechanism would not operate at 700 °C because Widmanstätten ferrite side plates were not observed at this temperature [1].

When the austenite became embedded in the ferrite, it adopted either an approximately spherical (Figs 2, 4a) or a faceted (Figs 1, 5b) morphology. A spherical shape will result when the austenite/ferrite interfacial energy is isotopic. This, in turn, could be taken as evidence that many of the austenite particles are bounded by high-energy incoherent interfaces. Conversely, the observation of faceting (Figs 1, 5b) implies that these latter particles are bounded, at least in part, by semicoherent interfaces. Hence, it is likely that both semi-coherent and incoherent interfaces are mobile during the decomposition of austenite in these alloys. In this context, the morphology of the austenite particle shown in Fig. 3a is of interest. It is suggested that low-energy semi-coherent interface with respect to grain A, is being replaced by higher energy, spherical interfaces in grain B.

4.2. The formation of ferrite/carbide aggregates

As noted in the previous section, for all times and temperatures for which austenite was still present, a significant fraction of the pools was still located on grain boundaries. Reference to Figs 6 and 7 shows that the large pools invariably transformed to pearlite during extended isothermal anneals. This is reasonable, in that there should be plenty of time for "co-operation" [10] to be established, after multiple nucleation events of cementite, on the austenite ferrite interface, has initiated the colony [1, 11]. For the smaller intergranular austenite pools, it is suggested that co-operation is never established and the nucleation of a single (or a small number of) cementite precipitate(s) can be sufficient to transform the entire pool of austenite. A schematic diagram of this event is presented in Fig. 13, which is a modification of that presented in Fig. 9. The major difference between the two decomposition routes is in Fig. 13c where it is assumed that cementite nucleates on the ferrite/austenite triple junction. This single carbide can grow by depleting the austenite pool in carbon and consequently the remaining pool transforms epitaxially to ferrite, leaving a cementite particle on the grain boundary. This precipitate can develop into a massive film, during prolonged holding at the isothermal transformation temperature, most probably by both coarsening and impingement with adjacent cementite precipitates. An example of a massive film of cementite that formed as described above, is given in Fig. 14. The two coalesced particles are labelled A and B.

The genesis of the observed intragranular cementite (Figs 6 and 7), is the intragranular pools of austenite which will finally transform to expitaxial ferrite plus cementite by a mechanism which is similar to that shown in Fig. 13c and d.

Finally, the distribution of cementite in Fig. 8 requires explanation. One obvious suggestion would be

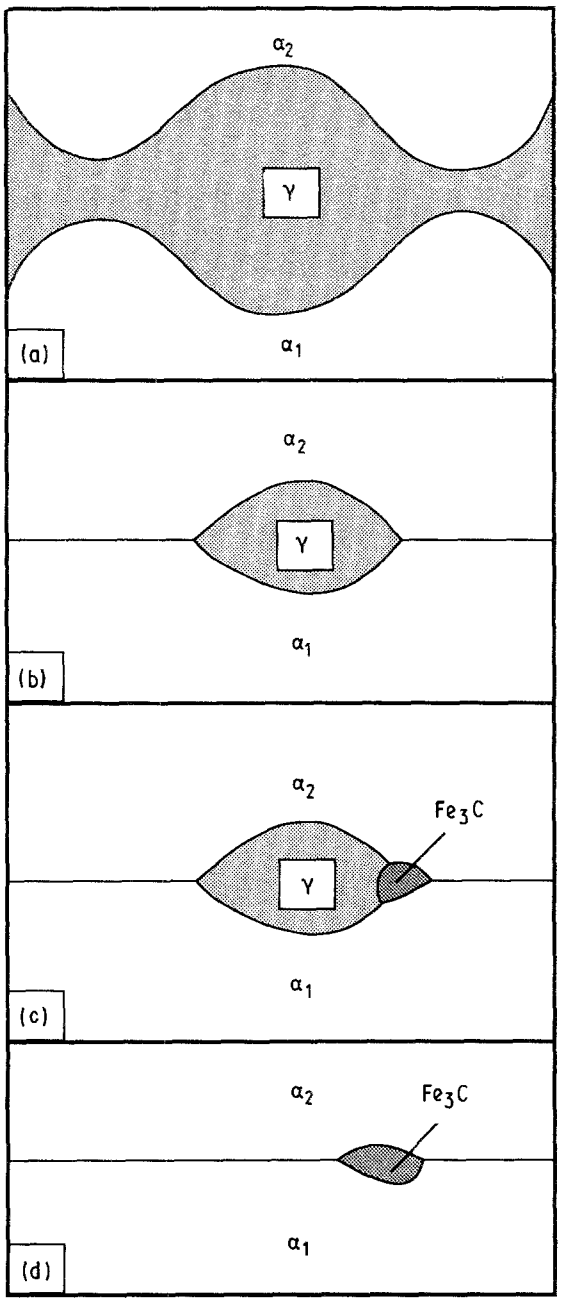

Figure 13 A schematic illustration of the formation of intergranular cementite. (a, b) As for Fig. 9. (c) Nucleation of cementite at the $\gamma/\alpha_1/\alpha_2$ triple junction. (d) Formation of grain-boundary cementite by epitaxial growth of α_1 and α_2 into the carbon-depleted austenite.

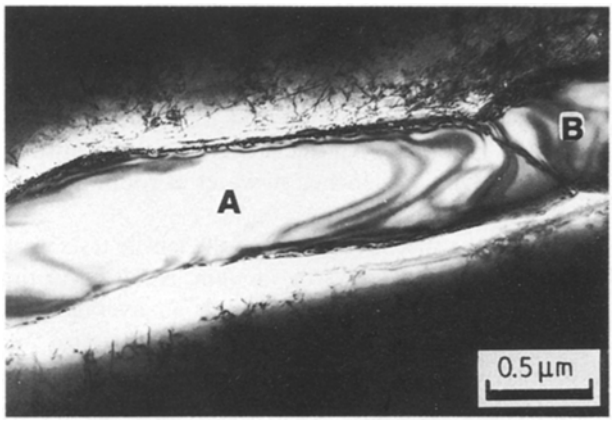

Figure 14 Transmission electron micrograph of a massive film of cementite at a ferrite grain boundary (Steel A, slowly cooled from the austenite range to room temperature).

that these precipitates formed by nucleation and growth at the ferrite grain boundaries and due to a residual carbon supersaturation. However, a more plausible explanation would involve the decomposition of austenite pools of a high aspect ratio. Such pools are seen, for example, in Figs 1, 10 and 11. Hence it is suggested that the puckering of the ferrite boundary in Fig. 8 is a post-transformation event, i.e. it occurs after impingement of the pearlite with the adjacent proeutectoid ferrite grain.

5. Conclusion

It has been found that the growth of proeutectoid ferrite in two low-carbon lamination steels partitions the austenite into a number of much smaller units. Ferrite grain growth proceeds and envelopment of many of the small austenite particles occurs. The large austenite pools on ferrite grain boundaries invariably transform to pearlite. However, the small intergranular pools yield discrete carbide particles upon transformation. These discrete precipitates of cementite can develop into massive films of cementite during prolonged holding at elevated temperatures. Finally, intragranular pools of austenite yield single cementite particles together with epitaxial ferrite.

Acknowledgements

Three of the authors (J.-W. L., S. W. T. and P. R. H.) thank the American Iron and Steel Institute and the Atlantic Richfield Foundation for the initial financial support. Subsequent financial support (for R. V. and P. R. H.) from The Office of Naval Research-Grant No. N00014-89-J1958 is also gratefully acknowledged. S. W. T. thanks the Advanced Steel Processing and Products Research Center, Colorado School of Mines for support. The authors are grateful to G. Ludkovsky, Inland Steel, Chicago, for the supply of specimen materials.

References

1. J.-W. LEE, S. W. THOMPSON and P. R. HOWELL, *J. Mater. Sci.* **25** (1990) 1699.
2. J. W. STEEDS, in "Introduction to Analytical Electron Microscopy", edited by J. J. Hren, J. I. Goldstein and D. C. Joy (Plenum Press, New York, 1979) p. 387.
3. C. ZENER, private communication to C. S. Smith, *TMS-AIME* **175** (1949) 15.
4. T. GLADMANN, *Proc. Roy. Soc. A* **294** (1966) 298.
5. J. M. RIGSBEE and P. J. VANDERAREND, in "Formable HSLA and Dual-Phase Steels", edited by A. T. Davenport (TMS-AIME, Warrendale, PA, 1979) p. 56.
6. B. V. N. RAO and M. S. RASHID, *Metallkde* **16** (1983) 19.
7. F. F. YI, K. J. YU, I. S. KIM and S. J. KIM, *Met. Trans.* **14A** (1983) 1497.
8. P-H CHANG, *Scripta Metall.* **18** (1984) 1245.
9. P. G. SHEWMON, "Transformations in Metals" (McGraw Hill, New York, 1969) p. 219.
10. M. HILLERT, in "Decomposition of Austenite by Diffusional Processes", edited by V. F. Zackay and H. I. Aaronson (Interscience, New York, 1962) p. 197.
11. S. W. THOMPSON and P. R. HOWELL, *Scripta Metall.* **22** (1988) 1775.

Received 28 January
and accepted 20 November 1992